RSC Advances

PAPER

View Article Online
View Journal | View Issue

Cite this: *RSC Adv.*, 2025, **15**, 37937

Influence of CO_2 substitution for N_2 on the combustion characteristics and kinetics of oil shale under oxy-fuel conditions

Qi Liu,[ab] Qing Wang,[*ab] Zhichao Wang[ab] and Huishuang Di[c]

Oxy-fuel combustion is recognized as a near-zero-emission technology and an effective route for large-scale CO_2 capture. Using TGA-DSC-MS, this study performed non-isothermal combustion tests on Fushun and Changji oil shales in two atmospheres—21%O_2/79%N_2 and 21%O_2/79%CO_2—to systematically assess how replacing N_2 with CO_2 alters combustion behavior and kinetic parameters. Across 0–1000 °C, the CO_2-containing atmosphere exhibits weaker momentum diffusion, heat transfer, and mass transport, which elevates ignition and burnout temperatures for both shales, delays the overall combustion process, and diminishes performance. The ignition and burnout stages of both materials are jointly governed by heating rate and CO_2 concentration. Furthermore, the addition of CO_2 causes the decomposition process of carbonates in Changji oil shale to shift from a single weight loss peak to three distinct peaks. Vyazovkin's advanced isoconversional kinetic analysis indicates that, as the combustion reaction progresses, the activation energy of both oil shales first decreases and then increases. In CO_2-enriched atmospheres, higher activation energy is required to complete the combustion process. The significant variation in combustion activation energy with conversion rate under both atmospheres demonstrates that the combustion of organic matter involves multiple parallel or sequential reactions, with the kinetic mechanism dynamically changing.

Received 28th July 2025
Accepted 30th September 2025

DOI: 10.1039/d5ra05471k

rsc.li/rsc-advances

1. Introduction

Since the Industrial Revolution, widespread fossil-fuel combustion has released substantial CO_2, driving atmospheric concentrations from 280 ppmv to over 420 ppmv in recent years.[1,2] To address this escalating challenge, China announced its "30–60" climate targets in 2020—peaking CO_2 emissions before 2030 and achieving carbon neutrality by 2060. Against this backdrop, transforming the high-carbon emissions profile of conventional fossil-fuel use has become imperative. China possesses abundant oil shale resources, with major deposits concentrated in regions such as Changji (Xinjiang) and Fushun (Liaoning). Changji's proven oil shale reserves reach 4.6 $\times$ 10^8 tons,[3] with a Type II kerogen.[4] Fushun's recoverable oil shale reserves reach 11 $\times$ 10^8 tons,[5] with a Type I and II kerogen.[6] Both Changji and Fushun oil shale coexist with coal, allowing the oil shale to be mined simultaneously during open-pit coal mining, resulting in low-cost extraction. Currently, both regions are being mined and utilized on a large-scale industrial scale. One of the primary applications of oil shale is combustion for power generation and heating.[7–9] Its development and utilization must align with low-carbon development goals. Accordingly, advancing efficient, clean combustion strategies for oil shale is both urgent and essential. Within this framework, oxy-fuel combustion offers a particularly promising pathway to markedly reduce CO_2 emissions associated with oil shale utilization.

Oxy-fuel combustion is widely regarded as an energy-efficient, cost-effective route for CO_2 reduction and capture. In this mode, fuel burns in a CO_2-rich environment, producing flue gas composed primarily of CO_2 and H_2O. Relative to conventional air firing, oxy-fuel operation yields a much higher CO_2 concentration in the exhaust and a markedly smaller flue-gas volume.[10–13] Pronounced contrasts between CO_2-rich and air atmospheres—spanning thermophysical properties, reaction pathways, and pollutant-formation behavior—have been documented. Building on these distinctions, extensive research has examined the combustion characteristics of solid fuels under oxy-fuel conditions.

Gil *et al.*[14] employed non-isothermal thermogravimetric analysis to examine the thermal reactivity of pulverized coal under oxy-fuel combustion conditions. The results indicated that substituting N_2 with CO_2 in a 21% O_2 atmosphere led to a reduction in the mass loss rate and caused a delay in the overall combustion process. Niu *et al.*[15] investigated the

[a]*School of Energy and Power Engineering, Northeast Electric Power University, Jilin, 132012, China. E-mail: rlx888@126.com*

[b]*Engineering Research Centre of Oil Shale Comprehensive Utilization, Ministry of Education, Northeast Electric Power University, Jilin, 132012, China*

[c]*School of Mechanical and Power Engineering, Shenyang University of Chemical Technology, Shenyang City, Liaoning, 110020, China*

combustion kinetics of three coal samples under oxy-fuel atmospheres, elucidating the influence of oxygen concentration on the combustion process. Their findings revealed that increasing O_2 levels from 10% to 40% enhances combustion, while beyond 40%, the effect tends to plateau. Within an oxygen concentration range of 10% to 60%, the activation energies of the samples varied between 111 kJ mol^{-1} and 317 kJ mol^{-1}. Liu *et al.*[16] examined the kinetics of coal char combustion under oxy-fuel conditions using a generalized surface activation function model. The study demonstrated that oxy-fuel substantially increases the char combustion rate and yields higher apparent activation energies than conventional air firing. Baqain *et al.*[17] investigated the ash characteristics produced during oxy-fuel combustion of Estonian oil shale. Their results indicate that oxy-fuel suppresses carbonate decomposition, while promoting the formation of secondary silicates and anhydrite, thereby altering the particle-size distribution and increasing the specific surface area of the ash. Loo *et al.*[18] investigated the combustion characteristics of Estonian oil shale under air and oxygen-enriched atmospheres using non-isothermal thermal analysis. Their findings indicated that the overall combustion rate increased with rising oxygen concentration. Notably, carbonate minerals in the oil shale decomposed in a single step under O_2/N_2 conditions, whereas under O_2/CO_2 atmospheres, the decomposition occurred *via* two distinct stages. Baqain *et al.*[19] employed TG-MS coupled with kinetic analysis to examine the co-combustion behavior of calcium-rich oil shale and biomass under air and oxy-fuel atmospheres. The results show that oxy-fuel co-firing alters combustion kinetics and gas emission profiles, with particularly pronounced effects on the release and transformation of volatile species. Bai *et al.*[20,21] utilized non-isothermal thermogravimetric analysis to investigate the combustion behavior and kinetic properties of Huadian oil shale under atmospheres of O_2/CO_2 and O_2/N_2. Their findings revealed that as the oxygen concentration increased from 10% to 50%, the combustion performance of the oil shale improved significantly, with a 30% O_2 and 70% CO_2 mixture identified as the most favorable for combustion. Owing to the heterogeneous composition of oil shale, the reaction mechanisms and kinetic parameters governing its oxy-fuel combustion are not yet fully resolved. Consequently, there is a clear need to delineate its combustion reactivity and kinetic behavior under both air and oxy-fuel conditions.

Various isoconversional methods have been applied in the literature to study the combustion kinetics of fuels such as oil shale. These methods include differential approaches, such as the Friedman method,[22] as well as integral methods, including Flynn–Wall–Ozawa,[23,24] Kissinger–Akahira–Sunose,[25,26] and Starink.[27] The Friedman method requires numerical differentiation, which amplifies the noise present in the experimental data. Additionally, smoothing the data introduces potential systematic errors into the kinetic parameters. The advantage of this method is that it does not require the evaluation of temperature integrals. Linear integral methods, such as FWO, KAS, and Starink, require simplifications of the temperature integral, necessitating the use of approximations. This can lead to significant errors when estimating activation energy.[28] Furthermore, these linear integral methods assume that activation energy remains constant across the entire integration range. In reality, the activation energy in the combustion process of solid fuels typically varies with conversion rate. Violating the assumption of constant activation energy introduces systematic errors. When the variation in activation energy with conversion rate is substantial, the relative error in activation energy can reach 20–30%.[29] To overcome the limitations of traditional kinetic analysis methods, the Kinetics Committee of the International Confederation for Thermal Analysis and Calorimetry (ICTAC)[30] recommends the use of the nonlinear integral method proposed by Vyazovkin.[31–33] This method avoids the use of temperature integral approximations by substituting temperature integration with time integration, thereby minimizing systematic errors associated with temperature integration. Additionally, the method assumes that the activation energy (E_α) remains constant only within a small α range (typically 0.01–0.02), which effectively eliminates errors caused by significant changes in E_α with α during the combustion of oil shale. The nonlinear integral method proposed by Vyazovkin has been widely recognized by many researchers.[34–36]

Previous work on oxy-fuel combustion has focused largely on coal and non-Chinese oil shales, with little in-depth analysis of Chinese deposits—particularly the representative Changji (Xinjiang) and Fushun (Liaoning) oil shales. In this study, these two shales were examined *via* non-isothermal combustion experiments under 21%O_2/79%N_2 and 21%O_2/79%CO_2 atmospheres to compare their combustion behavior and kinetic responses. Using coupled TGA-DSC-MS, we integrated mass loss, heat-flow, and gaseous product data to track characteristic changes in the combustion process (*e.g.*, ignition and burnout temperatures), thereby yielding more robust and informative conclusions. In addition, rather than conventional isoconversional approaches, we employed the more reliable advanced Vyazovkin method to determine the E_α–α relationship, enabling a deeper understanding of how activation energy and reaction mechanisms evolve during oil shale combustion. The findings furnish experimental evidence to optimize oxy-fuel utilization of oil shale and provide a theoretical basis for advances in clean combustion technologies.

2. Materials and methods

2.1. Materials

This study investigated two representative Chinese oil shales—Fushun (FS) and Changji (CJ)—both characterized by substantial reserves and active large-scale exploitation. The samples were crushed and milled to pass completely through a 100-mesh sieve, then dried in an oven at 40 °C to constant mass to remove external moisture. Subsequently, the dried materials were stored in a desiccator at ambient temperature to preserve sample integrity prior to analytical testing.

Table 1 reports the proximate and elemental analyses for the FS and CJ oil shales. Both exhibit ash contents >77%, volatile matter around 17%, and fixed carbon near 2%. These values

Table 1 Proximate analysis and ultimate analysis of Fushun oil shale and Changji oil shale[a]

	Proximate analysis (w_{ad} %)				Ultimate analysis (w_{ad} %)					
Oil shale	M	A	V	FC	C	H	N	O[a]	S_t[b]	HHV[c]
FS	2.15	77.26	17.93	2.66	12.35	2.37	0.82	4.52	0.53	4661
CJ	1.42	79.15	17.61	1.82	14.41	1.98	0.96	1.43	0.66	5223

[a] ad: air-dried basis; [a]: by difference; [b]: total sulfur; [c]: higher heating value, kJ kg^{-1}. M: moisture; A: ash; V: volatiles; FC: fixed carbon.

align with the commonly high ash and low fixed carbon characteristics of oil shale. Consistent with this composition, the two samples contain substantial mineral matter and relatively little combustible C and H, explaining their modest calorific values. The higher heating value (HHV) of CJ is 5223 kJ kg^{-1}, slightly exceeding that of FS (4661 kJ kg^{-1}). Sulfur levels are low in both cases, with contents <1%.

Table 2 reports the XRF-derived ash compositions of the two oil shales as oxide mass fractions (wt%). The ash is dominated by Si-, Al-, and Fe-bearing oxides, whose combined content exceeds 70 wt%. Minor constituents include Ca-, Mg-, K-, and Na-bearing oxides. A clear compositional contrast is observed: the FS sample contains markedly more Al-bearing oxides than CJ, whereas CJ exhibits a pronounced enrichment in Ca-bearing oxides. The remaining oxide components occur at broadly comparable levels in the two ashes.

2.2. Experimental apparatus and test conditions

Fuel combustion can be characterised using thermogravimetric analysis (TGA), a highly effective method.[37] This integrated thermal analysis enables simultaneous acquisition of mass loss, heat flow, time, and temperature, yielding TG and DSC curves. Experiments were performed on a Mettler–Toledo TGA/DSC1 with a sample mass of 10 ± 0.1 mg. The temperature was ramped from 30 to 1000 °C at programmed heating rates of 5, 10, 20, and 40 °C min^{-1}. Two carrier-gas mixtures were employed—21%O_2/79%N_2 and 21%O_2/79%CO_2—each supplied at a constant flow of 50 mL min^{-1}. The thermogravimetric analyzer was coupled to a Thermo Star mass spectrometer operating in multiple ion detection (MID) mode to characterize flue-gas composition in real time. Ion currents corresponding to CO_2 (m/z 44), H_2O (m/z 18), and O_2 (m/z 32) were continuously monitored, enabling time-resolved quantification of key gaseous species during oil shale combustion. Elemental composition analysis was carried out using a Bruker S8 TIGER X-ray fluorescence (XRF) spectrometer. The instrument is equipped with an X-ray tube featuring a rhodium (Rh) target, with a maximum power output of 4 kW, a peak voltage of 60 kV, a maximum current of 170 mA, and an angular resolution of 0.001°. To ensure the reproducibility of results, all measurements should be repeated at least twice.

Table 2 Compositional analysis of Fushun oil shale and Changji oil shale ashes (wt%)

Ash	SiO_2	Al_2O_3	Fe_2O_3	CaO	MgO	SO_3	TiO_2	K_2O	Na_2O	P_2O_5
FS	55.30	22.60	10.90	0.72	1.25	0.77	1.07	1.20	1.14	0.21
CJ	55.70	12.20	6.99	6.14	2.66	1.23	0.54	2.59	2.22	0.52

2.3. Method of determining combustion characteristic parameters

Thermogravimetric (TG) and derivative thermogravimetric (DTG) curves provide key thermal parameters for characterizing the combustion process, including the ignition temperature (T_i), burnout temperature (T_b), and the peak temperature (T_{max}) corresponding to the maximum weight loss rate. These thermal parameters serve as important indicators of the thermal decomposition behavior and reactivity of the organic components in oil shale, enabling a reliable evaluation of its combustion characteristics. In this study, the widely accepted TG-DTG tangent method was employed to determine the ignition temperature, with detailed procedures available in ref. 38. It is noteworthy that oil shale combustion typically yields multiple weight-loss peaks in the DTG profile. In this context, the ignition temperature is most appropriately defined as the first pronounced peak in the low-temperature region, reflecting the onset of volatile release followed by their oxidation.

The burnout temperature of solid fuels is commonly assessed using thermogravimetric analysis (TGA), wherein it is identified by achieving a weight loss rate below 1% per minute or by reaching 98% conversion, as reported in prior studies.[38–40] Oil shale commonly contains carbonate minerals that decompose at elevated temperatures during thermal analysis, producing mass loss unrelated to the combustion of organic matter. Accordingly, when determining the combustion temperature of the organic fraction from TGA data, the influence of carbonate decomposition must be accounted for. In this study, the conversion rate was adopted to identify the combustion temperature. Detailed analysis of the TG-DTG profiles indicated that the proportions of high-temperature decomposing minerals, such as carbonates, were approximately 7% in FS oil shale and 21% in CJ oil shale. As a result, the conversion rates corresponding to the combustion of organic matter were found to be 0.93 for FS and 0.79 for CJ oil shale, underscoring a pronounced difference between the two samples.

To evaluate the overall performance, the comprehensive combustion characterization index S of oil shale is employed in this paper, which is calculated as shown in eqn (1) and (2).[41] Researchers have extensively utilized the S index to investigate the combustion behavior of fuels under oxygen-enriched conditions. Its robustness in capturing combustion characteristics across diverse reaction environments has been rigorously demonstrated.[13,42–44]

$$S = \frac{R}{E}\frac{\mathrm{d}}{\mathrm{d}T}\left[\frac{\mathrm{d}w}{\mathrm{d}t}\right]_{T=T_i}\frac{(\mathrm{d}w/\mathrm{d}t)_{\max}}{(\mathrm{d}w/\mathrm{d}t)_{T=T_i}}\frac{(\mathrm{d}w/\mathrm{d}t)_{\mathrm{mean}}}{T_b} = \frac{(\mathrm{d}w/\mathrm{d}t)_{\max}(\mathrm{d}w/\mathrm{d}t)_{\mathrm{mean}}}{T_i^2 T_b} \quad (1)$$

$$(\mathrm{d}w/\mathrm{d}t)_{\mathrm{mean}} = (\alpha_{T_b} - \alpha_{T_i})/[(T_b - T_i)/\beta] \quad (2)$$

where $(\mathrm{d}w/\mathrm{d}t)_{\max}$, $(\mathrm{d}w/\mathrm{d}t)_{T=T_i}$ and $(\mathrm{d}w/\mathrm{d}t)_{\mathrm{mean}}$ are the maximum burning rate (% min^{-1}), the burning rate at the ignition tempera (min^{-1}), and the average rate of conversion of T_i to T_b (min^{-1}), respectively. β is the rate of temperature rise (K min^{-1}); T_b is the burnout temperature (K); T_i is the ignition temperature (K).

The integrated combustion characteristics index, S, R/E, is indicative of fuel activity. A smaller value of E corresponds to higher reactivity. The rate of change of combustion velocity at the ignition point, $[\mathrm{d}(\mathrm{d}w/\mathrm{d}t)\mathrm{d}T]_{T=T_i}$, is another important index. A larger value indicates a more violent ignition. $(\mathrm{d}w/\mathrm{d}t)_{\max}/(\mathrm{d}w/\mathrm{d}t)_{T=T_i}$ indicates the peak combustion velocity and the ignition combustion velocity ratio. $(\mathrm{d}w/\mathrm{d}t)_{\mathrm{mean}}/T_b$ indicates the ignition of the end of life. As the value of this ratio increases, so does the velocity of the burnout.

2.4. Kinetic analysis

An investigation was carried out to determine the combustion kinetic parameters of oil shale based on thermogravimetric analysis data. The study explored these parameters under two atmospheric conditions: one comprising 21% O_2 with 79% N_2, and the other consisting of 21% O_2 with 79% CO_2. The kinetic equation for the non-isothermal non-homogeneous phase reaction was based on the fundamental rate equation:

$$\frac{\mathrm{d}\alpha}{\mathrm{d}t} = k(T)f(\alpha) \quad (3)$$

In eqn (3), α represents the conversion rate of the experimental sample, t indicates the reaction time (in minutes), T signifies the reaction temperature (in Kelvin), $k(T)$ denotes the temperature-dependent reaction rate constant, and $f(\alpha)$ represents the reaction mechanism function. The conversion rate α is denoted as:

$$\alpha = \frac{m_0 - m_t}{m_0 - m_f} \quad (4)$$

In the experiment, m_0 is for the representation of the initial weights of the sample, while m_f is for the representation of the final weights. m_t is for the representation of the weight of the sample at a specific time. The aforementioned mass parameters are measured in milligrams (mg). Base on the Arrhenius equation, $k(T)$ can be written as:

$$k(T) = A\exp\left(-\frac{E}{RT}\right) \quad (5)$$

Bringing eqn (5) into eqn (3) yields eqn (6) below:

$$\frac{\mathrm{d}\alpha}{\mathrm{d}t} = A\exp\left(-\frac{E}{RT}\right)f(\alpha) \quad (6)$$

In the Arrhenius equation, the subscripts A represent the frequency factor (s^{-1}), E represent the activation energy (kJ mol^{-1}), and R represent the universal gas constant (8.314 J $(\mathrm{mol\ K})^{-1}$).

In the non-isothermal thermogravimetric analysis, the sample is heated at a constant rate, with a heating rate $\beta = \mathrm{d}T/\mathrm{d}t$ (K min^{-1}). Consequently, eqn (6) can be transformed as followed:

$$\frac{\mathrm{d}\alpha}{\mathrm{d}T} = \left(\frac{A}{\beta}\right)\exp\left(-\frac{E}{RT}\right)f(\alpha) \quad (7)$$

The combustion kinetics of oil shale were analyzed using eqn (7), which provides the study's principal framework. In oil-shale research, multi-rate thermogravimetric experiments are a standard means to quantify activation energy, typically in conjunction with an appropriate isoconversional analysis. This combined strategy has proven effective for extracting kinetic parameters from thermal data. Among available approaches, isoconversional methods are widely regarded as robust because they do not require *a priori* specification of the reaction model. These methods are generally classified as integral or differential; the integral class can be further divided into linear and nonlinear formulations. Traditional linear integration methods (FWO, KAS, and Starink, *etc.*) employ approximations for the temperature integral during substitution, which can result in substantial errors in the E_α, particularly when E_α varies significantly with the conversion rate.

In order to mitigate the errors associated with the conventional linear iso-conversional method, Vyazovkin[31–33] pioneered an advanced nonlinear integration procedure. This methodology operates under the assumption that the activation energy remains approximately constant over a short interval, with integration performed within this limited range as represented by eqn (8). For n experiments conducted at varying heating rates, the activation energy E_α for each discrete segment is determined by minimizing the function $\Phi(E_\alpha)$ defined in eqn (9). To establish the dependence of activation energy E_α on the conversion fraction α, this minimization procedure must be systematically repeated for each value of α. This method eliminates the need for approximation and solves for the temperature integral through the segmental integration of time, thus minimizing the systematic error associated with the temperature integral.[45]

$$J[E_\alpha,\ T_i(t_\alpha)] = \int_{t_{\alpha-\Delta\alpha}}^{t_\alpha}\exp\left(-\frac{E_\alpha}{RT_i(t)}\right)\mathrm{d}t \quad (8)$$

$$\Phi(E_\alpha) = \sum_{i=1}^{n}\sum_{j\neq 1}^{n}\frac{J[E_\alpha,\ T_i(t_\alpha)]}{J[E_\alpha,\ T_j(t_\alpha)]} \quad (9)$$

3. Results and discussion

3.1. Comparison of thermophysical parameters of two atmospheres

Combustion performance of solid fuels differs markedly between 21%O_2/79%CO_2 and 21%O_2/79%N_2 atmospheres, primarily because replacing N_2 with CO_2 substantially alters the

thermophysical properties of the medium. To quantify these contrasts at 1 atm, temperature-dependent thermophysical parameters were calculated for both gas mixtures. In addition, the distinct mass-diffusion behavior of O_2 in CO_2 *versus* N_2 affects oxygen transport to oil-shale particle surfaces during combustion. Accordingly, the mass-diffusion rates of 21% O_2 in 79% CO_2 and in 79% N_2 were computed over a range of temperatures. A consolidated summary of these results is provided in Table 3.

As shown in Fig. 1, the CO_2/N_2 ratios of kinematic viscosity (momentum diffusivity), thermal diffusivity, and mass diffusivity increase with temperature over 0–1000 °C but remain below unity. Thus, although contrasts diminish at higher temperatures, the CO_2-containing atmosphere consistently exhibits lower momentum, thermal, and mass diffusivities than its N_2-based counterpart, implying reduced heat- and mass-transfer capacity. The Prandtl number, which characterizes the coupling of thermal and velocity boundary layers ($Pr = \nu/\alpha = \mu C_p/k$), decreases monotonically during heating: the CO_2/N_2 Prandtl-number ratio falls from 1.03 at 0 °C to 0.96 at 1000 °C. This trend arises because the relative increase in thermal conductivity between the two atmospheres outpaces the corresponding rise in the C_p/μ ratio, yielding the observed decline.

3.2. Comparison of combustion characteristics under two atmospheres

3.2.1. Analysis of the overall combustion process. To evaluate the effect of replacing N_2 with CO_2 on oil shale combustion behavior, we conducted two series of programmed-temperature (non-isothermal) combustion experiments on the selected samples. Fig. 2 and 3 depict the TG and DTG curves for CJ and FS oil shale combusted in atmospheres containing 21% O_2 with either 79% N_2 or 79% CO_2, evaluated at heating rates of 5, 10, 20, and 40 °C min^{-1}. As summarized in Table 4, the two major mass loss peaks within the principal combustion stages of both oil shale samples under these conditions exhibit distinct characteristic parameters. Additionally, an increase in heating rate results in a clear displacement of the TG and DTG profiles toward higher temperature regions for both types of oil shale. The size of the specific offset can be found by looking at the highest temperature of the significant weight loss peak in the main combustion zone, as shown in Table 4. The phenomenon can be interpreted as follows: at a given temperature under programmed heating, a higher heating rate shortens the residence (reaction) time, yielding a larger residual mass at that temperature. Consequently, achieving the same extent of mass loss requires a higher temperature as the heating rate increases, producing a systematic shift of the TG and DTG curves toward higher temperatures during combustion.

Within 50–200 °C, both CJ and FS oil shales exhibit minor mass loss, primarily attributable to moisture evaporation. Prior studies similarly report moisture-related weight loss for air-dried oil shale between 60 and 200 °C,[46–48] reflecting the presence of clay minerals with crystallization water and adsorbed moisture that desorb at relatively low temperatures. As temperature rises, marked devolatilization/oxidation occurs for FS over 255–710 °C and for CJ over 260–770 °C in 21%O_2/79% N_2. Under 21%O_2/79%CO_2, the principal mass loss for FS shifts to 270–720 °C, whereas CJ displays substantial loss across 270–915 °C. Relative to the O_2/N_2 case, the dominant mass-loss intervals in O_2/CO_2 shift toward higher temperatures for both shales. This behavior can be rationalized by the reduced momentum diffusion, heat transfer, and mass transport capacities of CO_2-rich atmospheres, which require higher temperatures to achieve comparable reaction progress.

Under both atmospheric conditions, FS oil shale exhibited two prominent weight loss peaks in the DTG profiles. The first peak appeared within the temperature range of 333 to 400 °C, followed by a second peak between 464 and 509 °C. These mass loss events correspond well with the sequential processes of thermal decomposition of organic constituents, liberation and

Table 3 Physical properties of 21%O_2/79%N_2 and 21%O_2/79%CO_2 at 1 atm pressure[a]

Atmosphere	T °C	ρ kg m^{-3}	μ 10^{-5} kg (m s)$^{-1}$	ν 10^{-5} m^2 s^{-1}	C_p kJ (kg °C)$^{-1}$	C_v kJ (kg °C)$^{-1}$	k 10^{-2} W (m °C)$^{-1}$	α 10^{-4} m^2 s^{-1}	Pr —	$D_{O_2,X}$ 10^{-5} m^2 s^{-1}
21%O_2/79%N_2	0	1.289	1.72	1.33	1.012	0.722	2.40	0.184	0.724	1.75
	25	1.180	1.84	1.56	1.013	0.723	2.59	0.217	0.720	2.04
	200	0.743	2.60	3.50	1.032	0.743	3.77	0.492	0.711	4.52
	400	0.522	3.32	6.37	1.076	0.787	4.95	0.881	0.723	8.19
	600	0.403	3.96	9.82	1.123	0.835	6.01	1.330	0.739	12.66
	800	0.328	4.53	13.82	1.163	0.875	7.01	1.840	0.751	17.84
	1000	0.276	5.06	18.32	1.194	0.905	7.96	2.414	0.759	23.69
21%O_2/79% CO_2	0	1.829	1.50	0.82	0.843	0.636	1.70	0.110	0.743	1.29
	25	1.674	1.62	0.97	0.864	0.657	1.90	0.131	0.739	1.52
	200	1.052	2.44	2.32	0.990	0.785	3.33	0.320	0.726	3.48
	400	0.739	3.24	4.39	1.095	0.891	4.86	0.601	0.730	6.41
	600	0.569	3.93	6.90	1.169	0.965	6.27	0.941	0.733	9.99
	800	0.463	4.53	9.79	1.221	1.017	7.56	1.336	0.732	14.15
	1000	0.390	5.08	13.01	1.258	1.054	8.75	1.782	0.731	18.84

[a] T: temperature; ρ: density; μ: dynamic viscosity; ν: kinematic viscosity; C_p: isobaricheat capacity; C_v: isochoricheat capacity; k: thermal conductivity; α: thermal diffusivity; Pr: Prandtl number; $D_{O_2,X}$: mass diffusivity of O_2 in X.

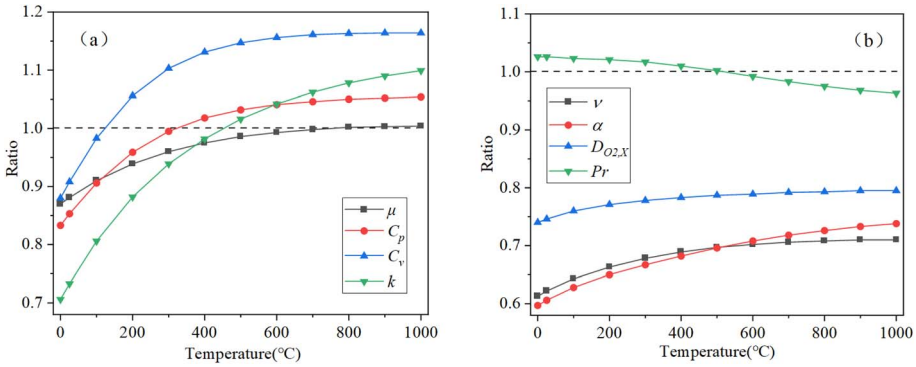

Fig. 1 The relationship between the ratio for physical properties of 21%O_2/79%CO_2 and 21%O_2/79%N_2 atmospheres and temperature at 1 atm pressure.

oxidation of volatile matter, and subsequent combustion of fixed carbon. Initial investigations into the combustion behavior of oil shale are consistent with the findings presented here.[49,50] The DTG profiles of Changji (CJ) oil shale under two different combustion atmospheres reveal distinct differences in thermal decomposition stages. Under the N_2-based atmosphere, three prominent weight loss peaks are observed, whereas combustion in a CO_2-containing atmosphere exhibits five distinct peaks. The first and second major peaks occur within the temperature ranges of 340–387 °C and 491–582 °C, respectively—values that are in close agreement with those recorded for Fushun (FS) oil shale. Under a 21%O_2/79%N_2 atmosphere, the third DTG peak of CJ oil shale appears at 646–732 °C and is attributed to CO_2 release from the thermal decomposition of carbonate minerals. In contrast, under 21% O_2/79%CO_2, the carbonate-related mass loss resolves into three distinct peaks: a third peak at 717–752 °C, a fourth at 790–807 °C, and a fifth at 873–890 °C. Relative to the N_2 case,

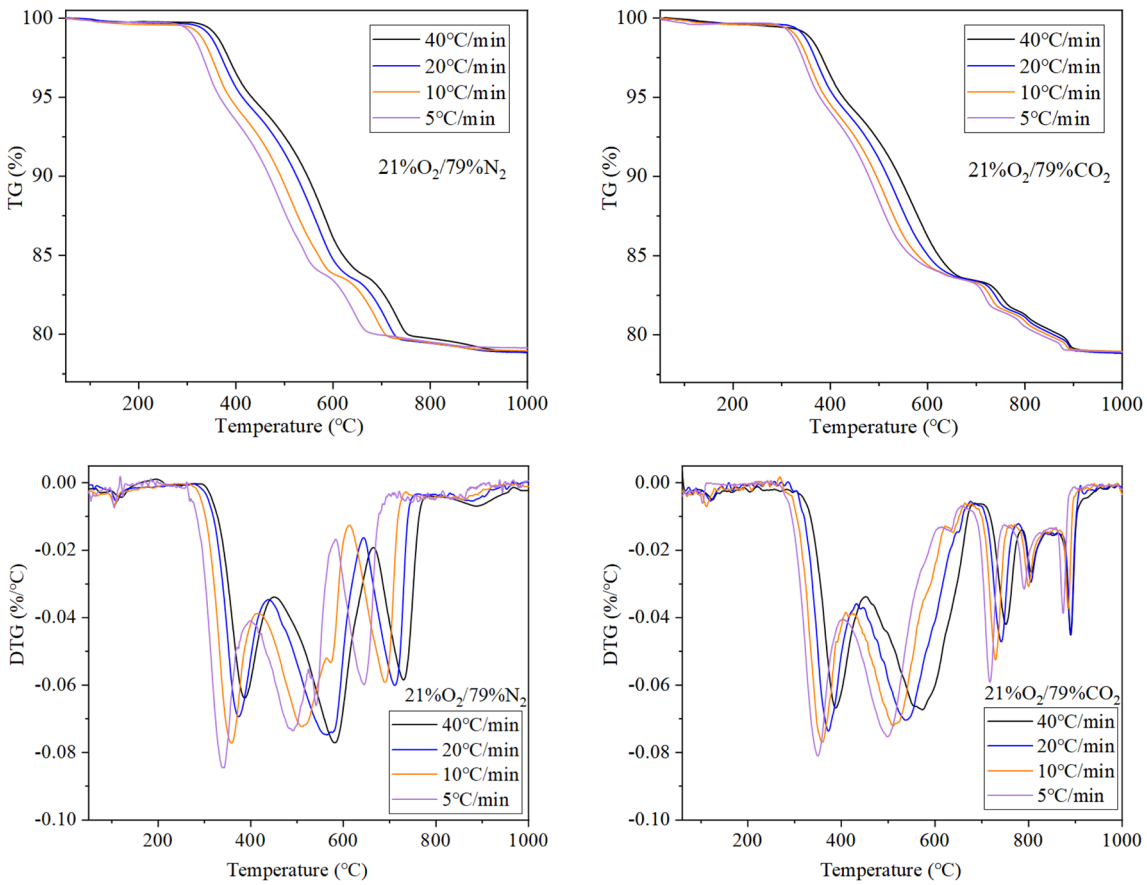

Fig. 2 TG and DTG curves of CJ oil shale combustion in the atmospheres of 21%O_2/79%CO_2 and 21%O_2/79%N_2.

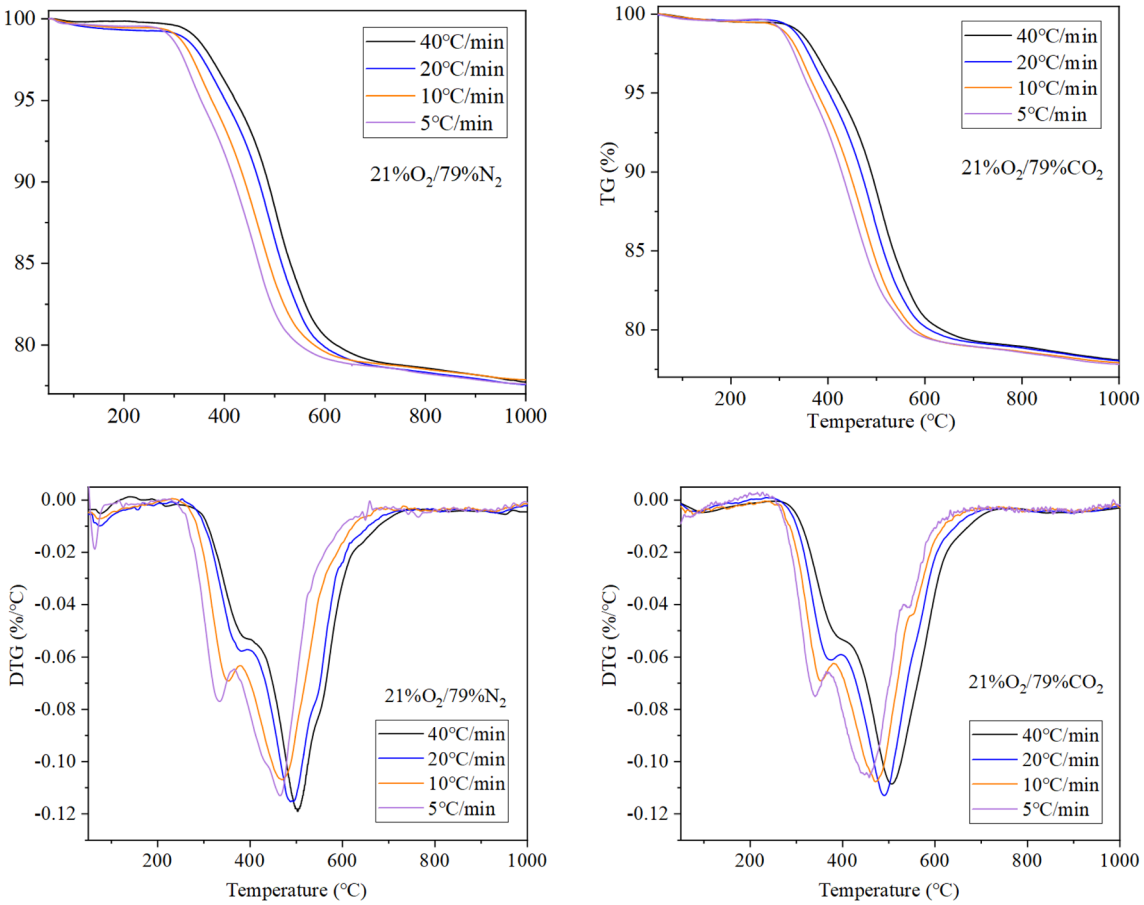

Fig. 3 TG and DTG curves of FS oil shale combustion in the atmospheres of 21%O_2/79%CO_2 and 21%O_2/79%N_2.

the carbonate decomposition features shift toward higher temperatures and evolve from a single event to three separate events when CO_2 replaces N_2 in the surrounding gas. Prior work on Estonian oil shale reported one carbonate decomposition peak in air but two in oxy-fuel conditions, corresponding to dolomite and calcite, respectively.[18] By analogy, the high-temperature peaks observed for CJ oil shale likely reflect successive decomposition of dolomite and calcite. The

Table 4 The peak characteristic parameters of CJ and FS oil shale combustion in 21%O_2/79%N_2 and 21%O_2/79%CO_2 atmospheres

Oil shale	Atmosphere	Heating rate β °C min^{-1}	T_{P1} °C	$(dw/dT)_{P1}$ % $°C^{-1}$	T_{P2} °C	$(dw/dT)_{P2}$ % $°C^{-1}$
CJ	21%O_2/79%N_2	5	342.8	−0.084	491.9	−0.073
		10	359.7	−0.077	513.3	−0.072
		20	373.6	−0.069	570.3	−0.074
		40	385.9	−0.063	582.4	−0.077
	21%O_2/79%CO_2	5	349.9	−0.081	497.4	−0.075
		10	360.5	−0.076	515.6	−0.072
		20	374.4	−0.073	539.8	−0.070
		40	389.4	−0.067	582.5	−0.067
FS	21%O_2/79%N_2	5	333.4	−0.077	464.1	−0.112
		10	353.7	−0.069	468.7	−0.107
		20	378.1	−0.057	490.3	−0.115
		40	398.1	−0.053	502.5	−0.117
	21%O_2/79%CO_2	5	341.9	−0.075	449.6	−0.105
		10	355.8	−0.069	473.4	−0.107
		20	379.6	−0.060	491.6	−0.110
		40	399.4	−0.053	508.3	−0.109

pronounced changes in CJ carbonate behavior across the two atmospheres indicate that the elevated CO_2 partial pressure in the CO_2-rich environment perturbs the decomposition equilibria, delaying carbonate breakdown. This delay separates processes that overlap in air into three distinct steps under high CO_2. A definitive assignment of the three peaks will be addressed in future work.

At a heating rate of 40 °C min^{-1}, the heat-flow traces of CJ and FS oil shales were acquired under two atmospheres. In both cases, two distinct exothermic events appear, with the high-temperature peak markedly weaker than the low-temperature one. These exotherms coincide with the principal mass-loss peaks within the main decomposition region of the DTG curves. Prior work indicates that the organic fraction of oil shale is dominated by aliphatic and aromatic compounds.[6] Accordingly, the low-temperature exotherm is ascribed to oxidation of H_2, CH_4, and CO released during the thermal cleavage of those structures, yielding a large amplitude and narrow width. The higher-temperature exotherm is primarily associated with oxidation of fixed carbon formed from aromatic condensation, and it exhibits a broader, lower-intensity peak. The overall profile further implies that, on a mass basis, hydrogen oxidation liberates more heat than carbon, consistent with the higher specific enthalpy of H_2 combustion.

Comparative evaluation of the two atmospheres indicates that the low-temperature exothermic peaks of both CJ and FS are of comparable magnitude, whereas the high-temperature exothermic peaks measured in 21%O_2/79%CO_2 are modestly attenuated. This attenuation is primarily attributable to the fact that the high-temperature exotherm arises from carbon oxidation to CO_2; an elevated ambient CO_2 level partially suppresses this reaction, thereby lowering peak intensity. By contrast, the low-temperature exotherm is dominated by combustion of hydrocarbon gases released during thermal decomposition of organic matter. Owing to the high concentration and reactivity of these species, this peak is far less sensitive to variations in the surrounding CO_2 concentration.

As highlighted by the boxed region in Fig. 4, CJ oil shale exhibits a distinct high-temperature endothermic peak under the N_2-containing atmosphere, consistent with the third mass-loss peak in the DTG trace. Under CO_2-containing conditions, three additional minor endothermic peaks appear, corresponding to the third through fifth DTG mass-loss events. The endothermic features in CJ's heat-flow curves under both atmospheres thus provide thermal evidence that the third to fifth DTG peaks originate from carbonate decomposition. By contrast, the FS sample shows no prominent high-temperature mass-loss peaks in the DTG curve and no discernible high-temperature endotherms in the heat-flow data, indicating a relatively low carbonate content.

3.2.2. Comparative analysis of combustion characteristic parameters. As shown in Fig. 5, the ignition (T_i) and burnout (T_b) temperatures of both CJ and FS oil shales increase with heating rate under both atmospheres. A higher rate shortens residence time at any given temperature, so higher temperatures are required to reach equivalent reaction extents. In the N_2-containing atmosphere, T_i rises by 51 °C (CJ) and 57 °C (FS), while T_b increases by 66 °C (CJ) and 76 °C (FS). In the CO_2-containing atmosphere, the corresponding increments are 41 °C (CJ) and 38 °C (FS) for T_i, and 69 °C (CJ) and 58 °C (FS) for T_b. Overall, the T_i and T_b responses are comparatively less sensitive to heating-rate changes in CO_2, a behavior attributable to the distinct thermal and diffusive properties of CO_2 relative to N_2.

As shown in Fig. 5, the ignition temperature (T_i) and burnout temperature (T_b) of both CJ and FS oil shale vary with changes in heating rate under the two examined atmospheric conditions. An increase in heating rate leads to a corresponding rise in T_i and T_b for both oil shale samples across both atmospheres. This is mainly because the heating rate has increased, meaning the samples need to reach higher temperatures to undergo the same chemical reactions. In the N_2-containing atmosphere, as the heating rate increased, T_i of CJ and FS oil shale increased by 51 °C and 57 °C, respectively, while T_b increased by 66 °C and 76 °C, respectively. In the CO_2-containing atmosphere, T_i of CJ and FS oil shale increased by 41 °C and 38 °C, respectively, while T_b increased by 69 °C and 58 °C, respectively. The findings suggest that, within an CO_2-containing atmosphere, T_i and T_b of oil shale are relatively insensitive to this change, a phenomenon primarily attributable to the thermal and diffusive properties of CO_2.

As shown in Fig. 5(a), under identical atmospheres and heating rates, the ignition temperature (T_i) of FS is lower than that of CJ. This implies weaker thermal stability of aliphatic structures in FS, promoting earlier thermal cleavage, release of flammable volatiles, and hence easier ignition. At 5 °C min^{-1}, the T_i values of both CJ and FS in N_2 are noticeably lower than in CO_2; however, the inter-atmosphere difference narrows with increasing heating rate, and the T_i values nearly converge at 40 °C min^{-1}. This trend indicates that, at higher heating rates, the influence of differing gas-phase thermophysical properties on ignition diminishes, and the heating rate becomes the dominant external factor governing T_i.

As shown in Fig. 5(b), under identical atmospheres and heating rates, FS exhibits a lower burnout temperature (T_b) than CJ, consistent with its earlier ignition and faster overall combustion. Here, "burnout temperature" refers specifically to the temperature at which the organic fraction is fully consumed; subsequent carbonate decomposition is excluded. With increasing heating rate, the inter-atmosphere difference in T_b at a given rate remains essentially constant, in contrast to the convergence observed for T_i. In the high-temperature burnout regime, differences in gas-phase thermophysical properties are less consequential, and the dominant process is oxidation of fixed carbon to CO_2. Elevated CO_2 partial pressure moderates this oxidation, necessitating higher temperatures to achieve complete burnout; this delaying effect persists across heating rates. Taken together, these results indicate that, among external factors, heating rate primarily governs T_i, whereas CO_2 concentration in the reaction atmosphere exerts the decisive control on T_b.

3.2.3. Integrated combustion characterization. Fig. 6 presents the comprehensive combustion characteristic index (S) for CJ and FS oil shales under CO_2- and N_2-containing atmospheres across a range of heating rates. The index S is a robust,

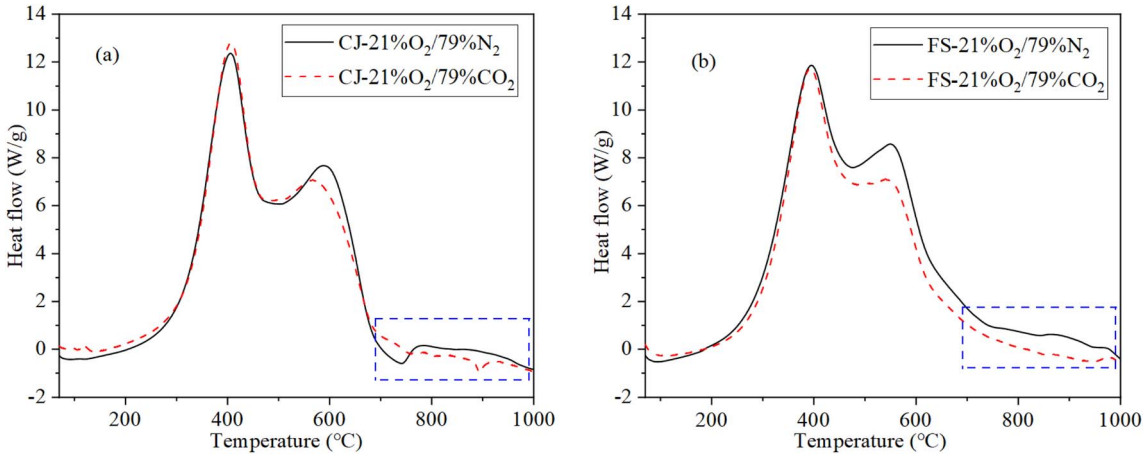

Fig. 4 Heat flow curve for CJ and FS oil shale combustion in the atmospheres of 21%O_2/79%CO_2 and 21%O_2/79%N_2 with heating rate of 40 °C min^{-1}.

integrated descriptor of the ignition, acceleration, and burnout stages of oil shale combustion. Higher S values signify improved overall combustion performance.

At a heating rate of 5 °C min^{-1}, the index S values for CJ and FS oil shale across both atmospheric conditions were found to range from 1.3×10^{-11} to 2.8×10^{-11}. At this point, the lower heating rate allows for sufficient reaction time under both atmospheres for CJ and FS oil shale, resulting in minimal differences in the effects of internal and external factors influencing the combustion process. As a result, the index S is analogous. With increasing heating rates, the index S of both CJ and FS oil shales shows a gradual increase, primarily due to the reduction in combustion time per unit temperature. The S index exhibits an approximately proportional relationship with the heating rate, which is consistent with the findings reported by Wang *et al.*[13]

Compared to the 21%O_2/79%CO_2 atmosphere, both CJ and FS oil shales exhibited higher S indices under the 21%O_2/79%N_2 atmosphere, indicating superior overall combustion performance in the latter condition. As the heating rate increases, the difference in S indices becomes more pronounced. This phenomenon can be attributed to the shortened reaction time at each temperature increment under higher heating rates, which amplifies the influence of differences in the combustion characteristics of internal organic matter as well as the thermophysical properties and CO_2 concentration of the surrounding atmosphere. Consequently, these factors lead to more significant variations in the S index.

At a given heating rate, the S index of FS is consistently higher than that of CJ under both atmospheres, in agreement with their respective ignition and burnout behaviors. These results indicate that, under identical conditions, FS exhibits more favorable overall combustion performance than CJ. The divergence primarily reflects intrinsic differences in organic matter composition and molecular architecture: FS kerogen is classified as Type I and II,[6] whereas CJ kerogen is Type II,[4] Consequently, FS shows a lower degree of metamorphism and a higher alkane content, which promotes easier ignition and more complete burnout, yielding a higher S index.

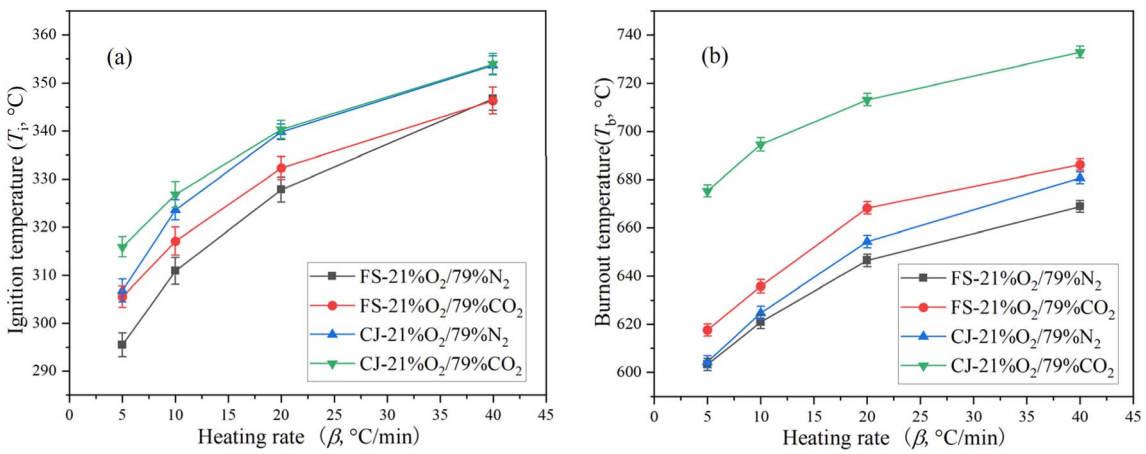

Fig. 5 Ignition temperature T_i and burnout temperature T_b for CJ and FS oil shale combustion in the atmospheres of 21%O_2/79%CO_2 and 21%O_2/79%N_2.

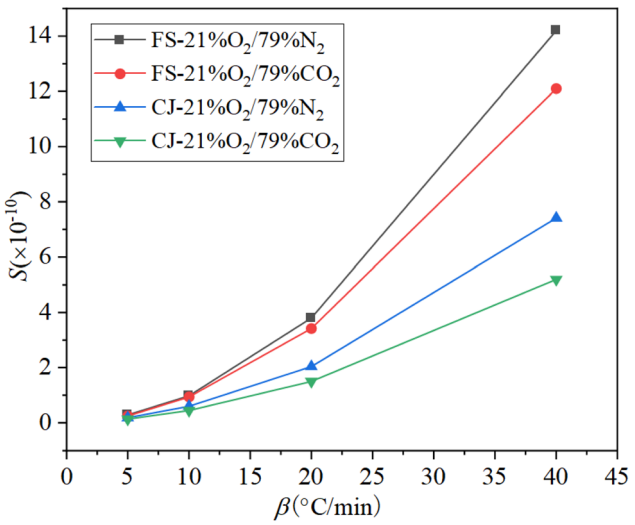

Fig. 6 Comprehensive combustion characteristics index S for CJ and FS oil shale combustion in the atmospheres of 21%O_2/79%CO_2 and 21%O_2/79%N_2.

3.3. Combustion kinetic analysis

The combustion behaviors of CJ and FS oil shale were systematically assessed under two different atmospheric environments. To facilitate this analysis, sophisticated iso-conversional methods, including the Vyazovkin method,[31–33] were utilized to elucidate the kinetics of the combustion reactions. As depicted in Fig. 7, the activation energy (E_α) associated with the combustion of organic matter in these oil shale samples exhibits a dependence on the conversion fraction (α) across both atmospheres studied. Importantly, α has been recognized as a dependable metric for characterizing the advancement of the combustion process.

In the context of two distinct atmospheric conditions, the activation energy E_α of CJ and FS oil shale demonstrate a tendency to initially decrease and subsequently increase in conjunction with the conversion rate α. This phenomenon is predominantly ascribed to the combustion reaction of oil shale organic matter, a process comprising multiple elementary reactions that occur in parallel, partially overlap, or sequentially. The kinetic mechanism of this process is subject to variation in conversion rate α, and this change is reflected in the activation energy as E_α. It is not possible for E_α to remain constant as α varies. The average activation energy for the combustion of CJ oil shale was calculated to be 179.3 kJ mol^{-1} under a CO_2-containing atmosphere and 124.3 kJ mol^{-1} under an N_2-containing atmosphere. In the case of FS oil shale, the corresponding values were 161.3 kJ mol^{-1} and 133.6 kJ mol^{-1}, respectively. These differences in activation energy between the two oil shale samples are primarily attributable to their distinct structural features and the varying presence of specific compositional constituents. The results of elemental analysis and other basic characteristic analyses in Section 2.2 of this paper indicate that there are certain differences in the organic matter and inorganic minerals within CJ and FS oil shale.

At the same α, E_α for the combustion of CJ and FS oil shale in a CO_2-containing atmosphere are notably higher than those observed in an N_2-containing environment. As demonstrated in Section 3.1 of this paper, when comparing the thermal properties of the two atmospheres (0–1000 °C), the momentum diffusion coefficient, thermal diffusion coefficient, and mass diffusion coefficient of the CO_2-containing atmosphere are all weaker than those of the N_2-containing atmosphere. As a result, in the CO_2-containing atmosphere, the diffusion of oxygen to the surfaces of oil shale particles, the particles' heating rates, and the surrounding gas turbulence are all reduced compared to conditions in the N_2-containing atmosphere. This results in more difficult combustion reactions in the CO_2-containing atmosphere, requiring more energy, as evidenced by the higher activation energy E_α required for combustion reactions.

Beyond α of 0.7 for CJ oil shale and 0.8 for FS oil shale, E_α for combustion rises more rapidly in the CO_2-containing atmosphere than in the N_2-containing atmosphere. The underlying reason for this phenomenon is that, within this conversion rate α interval, the combustion reaction is predominantly governed by fixed carbon combustion, with the combustion products being primarily CO_2. In the event of substituting 79% N_2 with

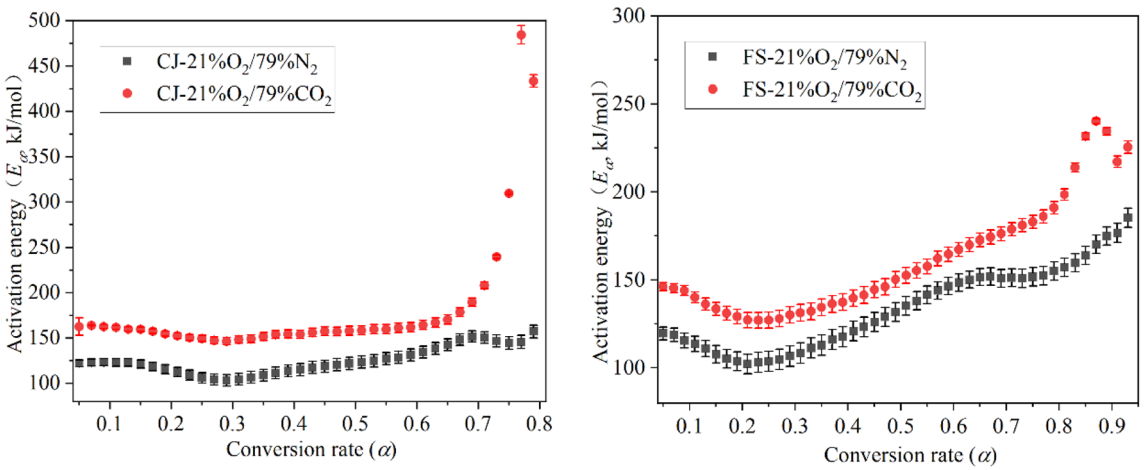

Fig. 7 Composite activation energy for CJ and FS oil shale combustion in the atmospheres of 21%O_2/79%CO_2 and 21%O_2/79%N_2.

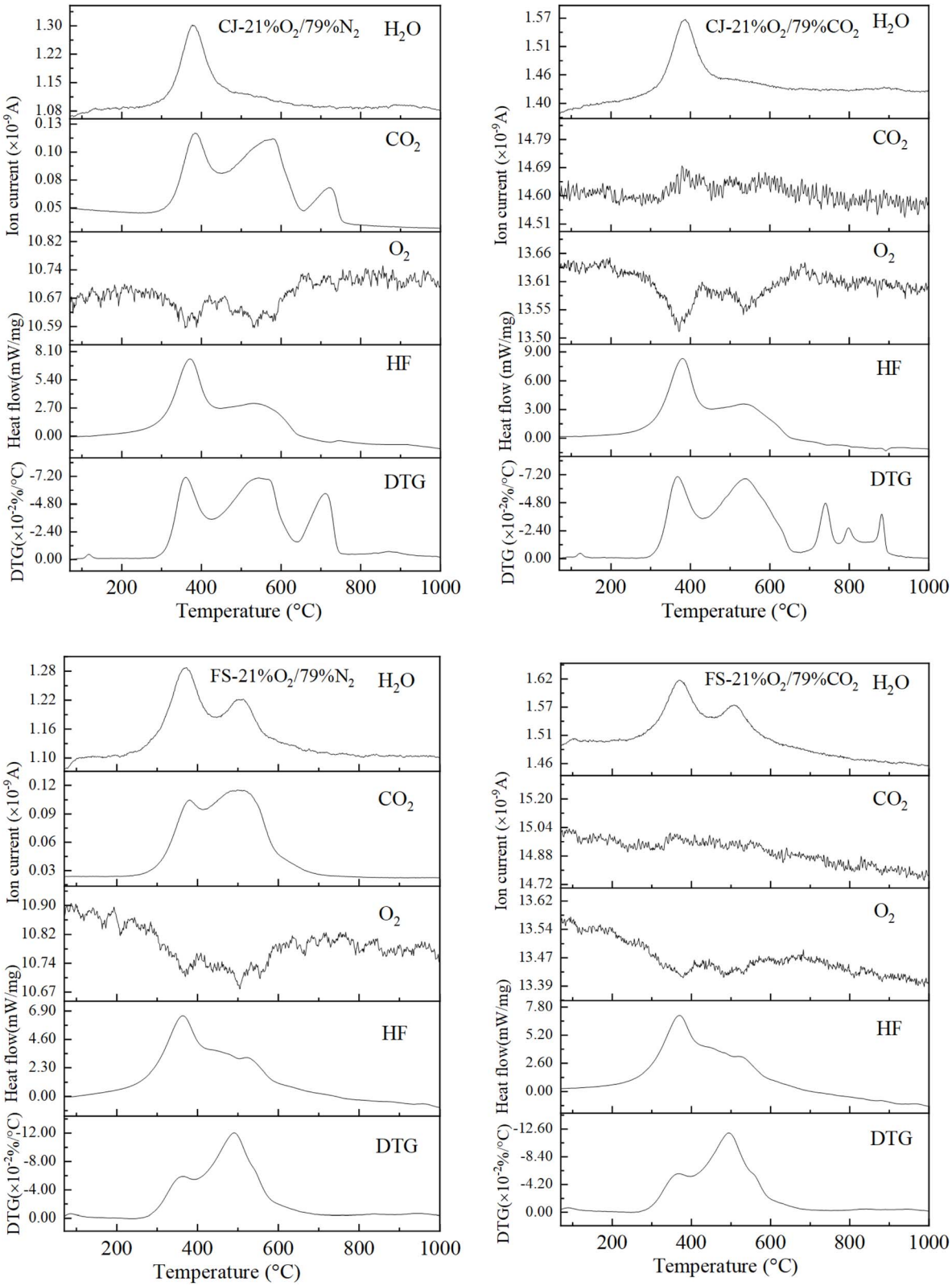

Fig. 8 O_2, CO_2 and H_2O evolution profiles followed by MS during CJ and FS oil shale combustion of 21%O_2/79%CO_2 and 21%O_2/79%N_2 (*m*/*z* 18, H_2O; *m*/*z* 32, O_2; *m*/*z* 44, CO_2, 20 °C min^{-1} heating rate).

79% CO_2 in the combustion atmosphere, there is a considerable increase in the partial pressure of CO_2 surrounding the fixed carbon. This, in turn, impedes the reaction of fixed carbon with O_2 to produce CO_2. Consequently, a greater quantity of energy is necessary to facilitate the combustion reaction, resulting in a substantial rise in E_α.

3.4. Combustion product analysis

As demonstrated in Fig. 8, the findings of mass spectrometry measurements of H_2O, CO_2, and O_2 in the emissions from the combustion of CJ and FS oil shales under the rate of 20 °C min^{-1} are presented. In both atmospheres, two generation peaks emerge on the ion flow curves of CO_2 and H_2O, while two consumption peaks appear on the O_2 curves during the combustion of CJ and FS oil shale. These observations correspond to the two weight loss peaks of organic matter combustion, indicating that organic matter combustion generates CO_2 and H_2O and consumes O_2.

In a 21%O_2/79%CO_2 atmosphere, the CO_2 signals from CJ and FS oil shales are attenuated, whereas in 21%O_2/79%N_2 they are more distinctly separated. This likely reflects masking of combustion-generated CO_2 by the elevated background CO_2 when N_2 is replaced, complicating resolution of the CO_2 evolution peak. Notably, for CJ in 21%O_2/79%N_2, a third CO_2-evolution peak appears at 650–760 °C, coincident with the third high-temperature mass-loss event in the DTG trace. These results indicate that CO_2 release is confined to a specific temperature window and corroborate that the third DTG peak in CJ arises from thermal decomposition of carbonate phases.

A salient finding is that, in both atmospheres, the first H_2O-evolution peak for CJ and FS exceeds the second, with the attenuation of the second peak especially pronounced for CJ. This behavior can be rationalized as follows. The initial mass-loss event predominantly reflects oxidation of hydrocarbon species generated by thermal cleavage of aliphatic structures, yielding relatively greater H_2O. The subsequent mass-loss event is governed by oxidation of aromatic constituents and fixed carbon, which produces less H_2O and proportionally more CO_2. Consistently, the primary exotherm in the heat-flow trace is substantially larger than the secondary one, providing thermal-signal corroboration of this interpretation.

4. Conclusions

This study employed TGA-DSC-MS to perform non-isothermal combustion experiments on Fushun and Changji oil shales under two atmospheres: 21%O_2/79%N_2 and 21%O_2/79%CO_2. The aim was to elucidate how replacing N_2 with CO_2 under oxy-fuel conditions affects combustion behavior and the associated kinetic parameters of these oil shales.

At a fixed O_2 concentration of 21%, the CO_2-containing atmosphere exhibits lower momentum (kinematic) diffusivity, thermal diffusivity, and mass diffusivity than its N_2-based counterpart across 0–1000 °C. Consequently, substituting N_2 with CO_2 diminishes both heat- and mass-transfer capacity. Relative to the N_2 atmosphere, both oil shales ignite and burn out at higher temperatures in CO_2, showing a clear delay in combustion and overall weaker performance, with the performance gap widening as the heating rate increases. For a given shale, the inter-atmosphere difference in ignition temperature progressively shrinks with increasing heating rate—indicating that heating rate becomes the dominant external factor at high rates—whereas the difference in burnout temperature remains nearly constant, underscoring the pivotal role of CO_2 concentration. Moreover, elevated CO_2 substantially affects carbonate decomposition in Changji oil shale, increasing the number of high-temperature DTG mass-loss peaks from one to three.

Vyazovkin isoconversional analysis—recognized for its robustness—indicates that both oil shales require higher apparent activation energies when combusted in CO_2-containing atmospheres. The oxidation of organic constituents in these samples is best described as a network of elementary reactions that may occur concurrently, partially overlap, or proceed sequentially, with the operative kinetic mechanism varying with conversion (α). In addition, the elevated background CO_2 in the oxy-fuel environment masks combustion-generated CO_2 in the mass-spectrometric signal, reducing the resolvability of the CO_2 ion-current peaks. This study provides empirical data and a theoretical basis for understanding how substituting CO_2 for N_2 alters the combustion characteristics and kinetic mechanisms of oil shale. For practical deployment, we recommend that the design of oxy-fuel oil shale boilers explicitly account for changes in heat and mass transfer, with corresponding optimization of furnace geometry and materials selection to ensure operational stability and efficiency.

Author contributions

Q. L.: methodology, investigation, data curation, visualization, and writing – original draft. Q. W.: conceptualization, funding acquisition and writing – review & editing. Z. W.: writing – review & editing. H. D.: writing – review & editing.

Conflicts of interest

There are no conflicts of interest to declare.

Data availability

The data supporting the conclusions of this study are available within the article. Additional datasets generated and analyzed during the current research can be obtained from the corresponding author upon request.

Acknowledgements

This research was supported by grants from the National Natural Science Foundation of China (No. 52476106).

References

1 K. Hashimoto, Global temperature and atmospheric carbon dioxide concentration, *Global Carbon Dioxide Recycling: for Global Sustainable Development by Renewable Energy*, Springer Singapore, Singapore, 2019, pp. 5–17.
2 W. J. Ripple, C. Wolf, J. W. Gregg, *et al.*, The 2024 state of the climate report: Perilous times on planet Earth, *BioScience*, 2024, **74**(12), 812–824.

3 Y. Lu, Y. Wang, J. Zhang, *et al.*, Co-combustion characteristics of Changji oil shale and coal, *Therm. Power Gener.*, 2019, **48**(04), 21–26.
4 Y. Lu, *Research on Pyrolysis and Combustion Characteristics of Jungdong Coal and Changji Oil Shale Mixtures and Their Kinetics*, Taiyuan University of Technology, 2020, pp. 33–34.
5 Y. Ma, Q. Y. Xiang and K. L. Ding, Development of oil shale at home and abroad, *World Pet. Ind.*, 2024, **31**(01), 16–25.
6 Q. Wang, Q. Liu, Z. C. Wang, *et al.*, Characterization of organic nitrogen and sulfur in the oil shale kerogens, *Fuel Process. Technol.*, 2017, **160**, 170–177.
7 S. Y. Li, Y. Ma and J. L. Qian, Global Oil Shale Research, Development and Utilization Today-And an Overview of Three Oil Shale Symposiums in 2011, *Sino-Global Energy*, 2012, **17**(02), 8–17.
8 E. Ozgur, S. F. Miller, B. G. Miller, *et al.*, Thermal analysis of co-firing of oil shale and biomass fuels, *Oil Shale*, 2012, **29**(2), 190–201.
9 T. Pihu, A. Konist, D. Neshumayev, *et al.*, Short-term tests on firing oil shale fuel applying low-temperature vortex technology, *Oil Shale*, 2012, **29**(1), 3–17.
10 F. Châtel-Pélage, R. Varagani, P. Pranda, *et al.*, Applications of oxygen for NOx control and CO_2 capture in coal-fired power plants, *Therm. Sci.*, 2006, **10**(3), 119–142.
11 Y. Tan, E. Croiset, M. A. Douglas, *et al.*, Combustion characteristics of coal in a mixture of oxygen and recycled flue gas, *Fuel*, 2006, **85**(4), 507–512.
12 M. B. Toftegaard, J. Brix, P. A. Jensen, *et al.*, Oxy-fuel combustion of solid fuels, *Prog. Energy Combust. Sci.*, 2010, **36**(5), 581–625.
13 C. A. Wang, X. Zhang, Y. Liu, *et al.*, Pyrolysis and combustion characteristics of coals in oxyfuel combustion, *Appl. Energy*, 2012, **97**, 264–273.
14 M. V. Gil, J. Riaza, L. álvarez, *et al.*, A study of oxy-coal combustion with steam addition and biomass blending by thermogravimetric analysis, *J. Therm. Anal. Calorim.*, 2012, **109**(1), 49–55.
15 S. Niu, C. Lu, K. Han, *et al.*, Thermogravimetric analysis of combustion characteristics and kinetic parameters of pulverized coals in oxy-fuel atmosphere, *J. Therm. Anal. Calorim.*, 2009, **98**(1), 267–274.
16 Y. Liu, Z. Shi, K. Li, *et al.*, Study on intrinsic reaction kinetics of coal char oxy-fuel combustion based on general surface activation function model, *Combust. Flame*, 2025, **273**, 113952.
17 M. Baqain, C. R. Yörük, D. Neshumayev, *et al.*, Ash characterisation formed under different oxy-fuel circulating fluidized bed conditions, *Fuel*, 2023, **338**, 127244.
18 L. Loo, B. Maaten, A. Siirde, *et al.*, Experimental analysis of the combustion characteristics of Estonian oil shale in air and oxy-fuel atmospheres, *Fuel Process. Technol.*, 2015, **134**, 317–324.
19 M. Baqain, D. Neshumayev and A. Konist, TG-MS analysis and kinetic study of co-combustion of ca-rich oil shale with biomass in air and oxy-like conditions, *Carbon Capture Sci. Technol.*, 2024, **10**, 100162.
20 F. Bai, Y. Sun and Y. Liu, Thermogravimetric analysis of Huadian oil shale combustion at different oxygen concentrations, *Energy Fuels*, 2016, **30**(6), 4450–4456.
21 F. Bai, J. Zhao and Y. Liu, An investigation into the characteristics and kinetics of oil shale oxy-fuel combustion by thermogravimetric analysis, *Oil Shale*, 2019, **36**(1), 1–18.
22 H. L. Friedman, Kinetics of thermal degradation of char-forming plastics from thermogravimetry. Application to a phenolic plastic, *J. Polym. Sci. C Polym. Lett.*, 1964, **6**(1), 183–195.
23 J. H. Flynn and L. A. Wall, A quick, direct method for the determination of activation energy from thermogravimetric data, *J. Polym. Sci. B Polym. Lett.*, 1966, **4**(5), 323–328.
24 T. Ozawa, A new method of analyzing thermogravimetric data, *Bull. Chem. Soc. Jpn.*, 1965, **38**(11), 1881–1886.
25 H. E. Kissinger, Reaction kinetics in differential thermal analysis, *Anal. Chem.*, 1957, **29**(11), 1702–1706.
26 T. Akahira and T. Sunose, Method of determining activation deterioration constant of electrical insulating materials, *Res. Rep. Chiba Inst. Technol.*, 1971, **16**, 22–31.
27 M. J. Starink, The determination of activation energy from linear heating rate experiments: a comparison of the accuracy of isoconversion methods, *Thermochim. Acta*, 2003, **404**(1–2), 163–176.
28 N. Sbirrazzuoli, Is the Friedman method applicable to transformations with temperature dependent reaction heat?, *Macromol. Chem. Phys.*, 2007, **208**(14), 1592–1597.
29 S. Vyazovkin, *Isoconversional Kinetics of Thermally Stimulated Processes*, Springer, 2015.
30 S. Vyazovkin, A. K. Burnham, J. M. Criado, *et al.*, ICTAC Kinetics Committee recommendations for performing kinetic computations on thermal analysis data, *Thermochim. Acta*, 2011, **520**(1–2), 1–19.
31 S. Vyazovkin and D. Dollimore, Linear and nonlinear procedures in isoconversional computations of the activation energy of nonisothermal reactions in solids, *J. Chem. Inf. Comput. Sci.*, 1996, **36**(1), 42–45.
32 S. Vyazovkin, Evaluation of activation energy of thermally stimulated solid-state reactions under arbitrary variation of temperature, *J. Comput. Chem.*, 1997, **18**(3), 393–402.
33 S. Vyazovkin, Modification of the integral isoconversional method to account for variation in the activation energy, *J. Comput. Chem.*, 2001, **22**(2), 178–183.
34 R. Ochieng, A. L. Cerón, A. Konist, *et al.*, A combined analysis of the drying and decomposition kinetics of wood pyrolysis using non-isothermal thermogravimetric methods, *Energy Convers. Manage.: X*, 2023, **20**, 1–12.
35 G. Lérys and N. Sbirrazzuoli, Isoconversional Computations for Nonisothermal Kinetic Predictions, *Thermochim. Acta*, 2021, **697**(1), 178859.
36 N. Sbirrazzuoli, Model-free isothermal and nonisothermal predictions using advanced isoconversional methods, *Thermochim. Acta*, 2020, **697**(3), 178855.
37 M. A. Islam, M. Auta, G. Kabir, *et al.*, A thermogravimetric analysis of the combustion kinetics of karanja (Pongamia pinnata) fruit hulls char, *Bioresour. Technol.*, 2015, **200**, 335.

38 J. J. Lu and W. H. Chen, Investigation on the ignition and burnout temperatures of bamboo and sugarcane bagasse by thermogravimetric analysis, *Appl. Energy*, 2015, **160**, 49–57.

39 S. Niu, K. Han and C. Lu, Characteristics of coal combustion in oxygen/carbon dioxide atmosphere and nitric oxide release during this process, *Energy Convers. Manage.*, 2011, **52**(1), 532–537.

40 Q. Li, C. Zhao, X. Chen, *et al.*, Comparison of pulverized coal combustion in air and in O_2/CO_2 mixtures by thermogravimetric analysis, *J. Anal. Appl. Pyrolysis*, 2009, **85**(1–2), 521–528.

41 X. M. Jiang, J. B. Li and J. R. Qiu, Study on combustion characteristics of superfine pulverized coal, *Proc. CSEE*, 2000, (06), 72–75+79.

42 Y. S. Fan, Z. Zou, J. B. Gao, *et al.*, Study of oxygen content on combustion characteristics of pulverized coal, *Proc. CSEE*, 2005, **25**(24), 118–121.

43 Q. Z. Li and C. S. Zhao, Investigation on characteristics of pulverized coal combustion in O_2/CO_2 mixtures, *Proc. CSEE*, 2007, **27**(35), 39–43.

44 M. Lei, C. B. Wang, P. Yan, *et al.*, Thermogravimetric research on pressurized oxy-fuel combustion of Datong bituminous coal, *Proc. CSEE*, 2012, **32**(05), 21–26.

45 S. Vyazovkin, Model-free kinetics: staying free of multiplying entities without necessity, *J. Therm. Anal. Calorim.*, 2006, **83**, 45–51.

46 A. J. Berkovich, J. H. Levy, S. J. Schmidt, *et al.*, Heat capacities and enthalpies for some Australian oil shales from non-isothermal modulated DSC, *Thermochim. Acta*, 2000, **357**, 41–45.

47 J. O. Jaber and S. D. Probert, Non-isothermal thermogravimetry and decomposition kinetics of two Jordanian oil shales under different processing conditions, *Fuel Process. Technol.*, 2000, **63**(1), 57–70.

48 Z. Wang, S. Deng, Q. Gu, *et al.*, Pyrolysis kinetic study of Huadian oil shale, spent oil shale and their mixtures by thermogravimetric analysis, *Fuel Process. Technol.*, 2013, **110**, 103–108.

49 M. F. Martins, *et al.*, Co-current combustion of oil shale-Part 2: Structure of the combustion front, *Fuel*, 2010, **89**(1), 133–143.

50 B. A. M. Zanoni, H. Massard and F. M. Martins, Formulating and optimizing a combustion pathway for oil shale and its semi-coke, *Combust. Flame*, 2012, **159**(10), 3224–3234.